Journal of Sound and Vibration 329 (2010) 2276–2290

Contents lists available at ScienceDirect

Journal of Sound and Vibration

journal homepage: www.elsevier.com/locate/jsvi

Prediction of the acoustic pressure above periodically uneven facings in industrial workplaces

J. Ducourneau [a,*], L. Bos [a], V. Planeau [b], Adil Faiz [a], Salah Skali Lami [c], A. Nejade [b]

[a] Laboratoire de Bio mathématique et Audioprothèse, Faculté de Pharmacie, Université Henri Poincaré, 5, rue Albert Lebrun, 54001 Nancy, France
[b] Institut National de Recherche et Sécurité, Avenue de Bourgogne, 54501 Vandœuvre-lès-Nancy, France
[c] Laboratoire d'Energétique et de Mécanique Théorique et Appliquée, 2, avenue de la Forêt de Haye, BP160, 54504 Vandœuvre-lès-Nancy Cedex, France

ARTICLE INFO

Article history:
Received 30 January 2009
Received in revised form
22 December 2009
Accepted 22 December 2009
Handling Editor: A.V. Metrikine
Available online 21 January 2010

ABSTRACT

The aim of this work is to predict sound pressure in front of wall facings based on periodic sound scattering surface profiles. The method involves investigating plane wave reflections randomly incident upon an uneven surface. The waveguide approach is well suited to the geometries usually encountered in industrial workplaces. This method simplifies the profile geometry by using elementary rectangular volumes. The acoustic field in the profile interstices can then be expressed as the superposition of waveguide modes. In past work, walls considered are of infinite dimensions and are subjected to a periodic surface profile in only one direction. We therefore generalise this approach by extending its applicability to "double-periodic" wall facings. Free-field measurements have been taken and the observed agreement between numerical and experimental results supports the validity of the waveguide method.

1. Introduction

Acoustic characterisation of surfaces in industrial workplaces is required for predicting the sound pressure level at specific points, improving the acoustic treatment and providing suitable noise control solutions in these environments. Periodic uneven sound scattering surfaces are often present in industrial workplaces. Fig. 1 shows an example of 1D periodic uneven surface defined by the sinusoidal profile $y=\zeta(x)$ and by the specific acoustic admittance on the surface $\eta=\eta(x)$.

In 1907, Rayleigh [1] solved the problem of the reflection of a time-harmonic plane wave, normally incident on an uneven surface of sinusoidal profile of small thickness (Fig. 1). Since then, many works [2–5] on sound reflection from sinusoidal profiles have used Rayleigh's method. However, Rayleigh's hypothesis is now considered as adaptable only to sinusoidal profiles with small depth. To consider Rayleigh's method as valid, the period L_x and the depth h of the profile, defined by the function, $y=\zeta(x)$ must satisfy the condition $2\pi h/L_x<0.6627$. The Rayleigh method is especially suited to flat surfaces with periodic acoustic admittance [6].

Based on the Dirichlet boundary conditions, Holford [5] proposed in 1981 an exact solution to the reflection of obliquely incident plane waves striking an infinite periodic profile. Holford's investigations are based on those of Urusovskii [7] involving periodic surfaces with uniform boundary conditions. Random-incidence scattering coefficients obtained by measurement in reverberation chambers for a particular sine-shaped surface have been compared with the Holford–Urusovskii's method [8].

* Corresponding author. Tel.: +33 3 83 68 23 43.
E-mail address: Joel.Ducourneau@pharma.uhp-nancy.fr (J. Ducourneau).

0022-460X/$ - see front matter © 2010 Elsevier Ltd. All rights reserved.
doi:10.1016/j.jsv.2009.12.028

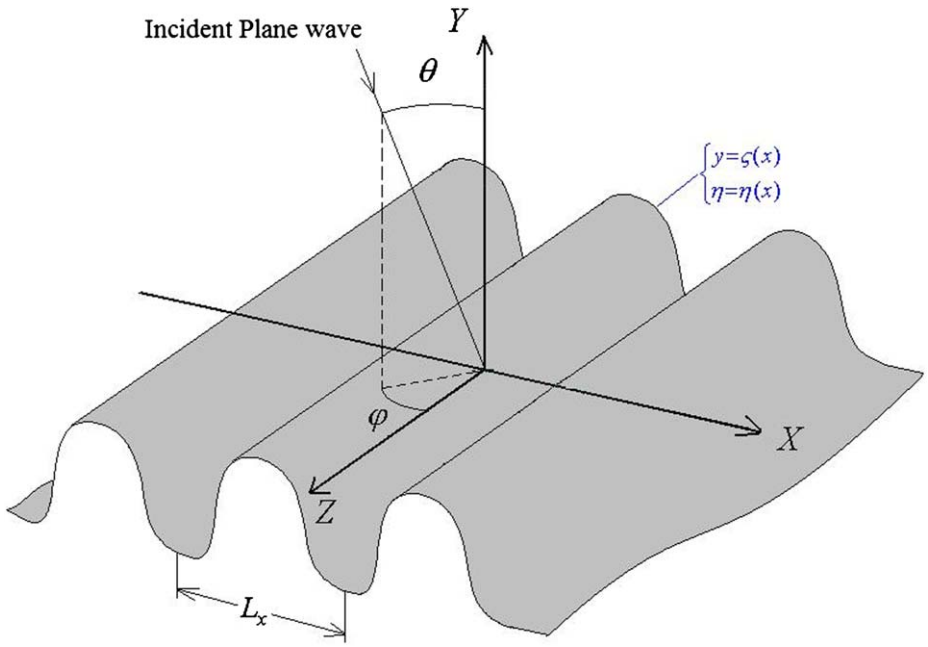

Fig. 1. 1D periodic uneven surface of sinusoidal profile.

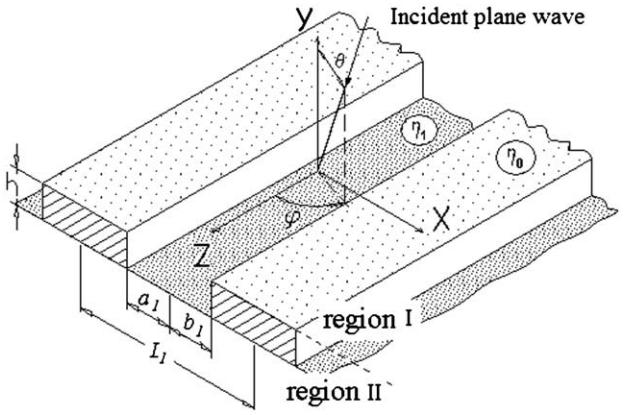

Fig. 2. 1D periodic uneven surface of rectangular profile with absorbent grooves.

Both Fujimoto and Fujiwara [9], and Lam [10] used the boundary element method to determine the amplitudes R_r of a reflected wave on periodic profiles. We note that Fujimoto and Fujiwara's method is adapted to more complex profile types, such as those encountered in industrial workplaces.

The finite element method [11] used by Macey [12] also determines the amplitudes R_r of reflected waves. This method is less efficient than the boundary element method because it requires higher spatial resolution, especially in the profile interstices.

In 1952, Deryugin [13] studied the case of a 1D periodic uneven surface with rectangular, non-absorbent grooves. In 1967, De Bruijn [14] used Deryugin's method to study the reflection of a plane wave incident randomly, on a surface with absorbent grooves, as shown in Fig. 2. Then, Ando and Kato [15] transposed the method for 1D periodic uneven surfaces of arbitrary profiles.

The present work is an extension of De Bruijn's model. It concerns the characterisation of 2D periodic uneven surfaces of infinite dimensions made of rectangular cavities. The aim is to determine the acoustic pressure in front of this kind of wall facing at a specific point.

Many 2D periodic uneven surfaces can be found in industrial workplaces. They could be composed of several superposed rectangular waveguides.

In what follows, d_{x_i} and d_{z_i} are the transversal dimensions of the ith rectangular waveguide in x and z coordinates, respectively. The corresponding lower and upper limits are a_{x_i} and b_{x_i}, along the x-axis, and a_{z_i} and b_{z_i}, along the z-axis.

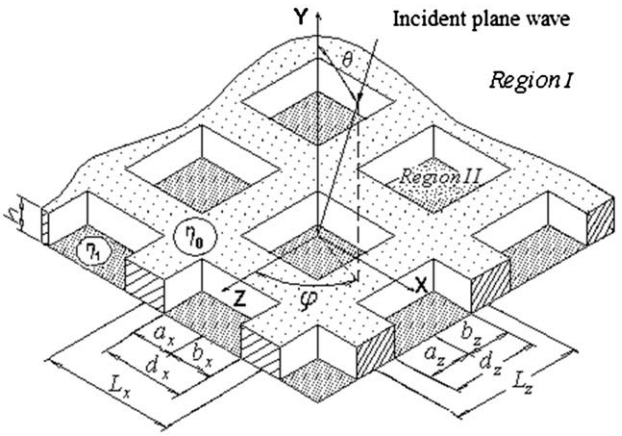

Fig. 3. 2D periodic uneven surface of rectangular profile.

For the profile A, both ith and $(i+1)$th rectangular waveguide coordinates satisfy the equation given below:

$$|a_{x_i}| > |a_{x_{i+1}}|, \quad a_{z_i}| > |a_{z_{i+1}}|, \quad b_{x_i} > b_{x_{i+1}}, \quad b_{z_i} > b_{z_{i+1}}. \tag{1}$$

For the profile B:

$$|a_{x_i}| < |a_{x_{i+1}}|, \quad |a_{z_i}| < |a_{z_{i+1}}|, \quad b_{x_i} < b_{x_{i+1}}, \quad b_{z_i} < b_{z_{i+1}}. \tag{2}$$

Figs. 4 and 5 show, respectively, two examples of periodic uneven surfaces of profiles A and B with two superposed waveguides ($i=1$):

- For profile A (cf. Fig. 4): $|a_{x_1}| > |a_{x_2}|, \quad |a_{z_1}| > |a_{z_2}|, \quad b_{x_1} > b_{x_2}, \quad b_{z_1} > b_{z_2}$.
- For profile B (cf. Fig. 5): $|a_{x_1}| < |a_{x_2}|, \quad |a_{z_1}| < |a_{z_2}|, \quad b_{x_1} < b_{x_2}, \quad b_{z_1} < b_{z_2}$

Fig. 6 shows the geometric cross section of these two profiles.

We study here the reflected acoustic field above 2D periodic surfaces made only of one (Fig. 3) or two superposed waveguides (Fig. 4 or 5).

2. Analysis of 2D periodic uneven surfaces with *N* waveguides

As suggested by De Bruijn's method [14] for 1D periodic uneven surfaces, we consider two regions of the space, the first one in front of the wall facing, referred to as region I and the second, inside the wall cavities, referred to as region II.

The cavity ridges of the periodic wall facing studied are considered acoustically rigid, while the faces perpendicular to y-axis may be covered with absorbing materials.

The generalisation involving N waveguides for 1D periodic surface profiles, introduced by Ando and Kato [15], is also applicable to 2D periodic profiles. Based on the notations used in Figs. 4–6, every waveguide referenced by the index i is bound by coordinates a_{x_i} and b_{x_i} along the x-axis and a_{z_i} and b_{z_i} along the z-axis. Its transverse dimensions are $d_{x_i} = b_{x_i} - a_{x_i}$ and $d_{z_i} = b_{z_i} - a_{z_i}$ and its depth is $h_i - h_{i-1}$.

Different geometries can be encountered, depending on whether the transverse dimensions d_{x_i} and d_{z_i} and the positions $a_{x_i}, a_{z_i}, b_{x_i}$ and b_{z_i} of the waveguide i are greater or smaller than those of the guide $i+1$. We decided to examine two cases corresponding to the two geometric shapes shown in Fig. 4 (profile A) and Fig. 5 (profile B).

In addition to the surface profile geometric variation, each side-step i can be covered with an absorbing material characterised by its specific acoustic admittance η_i. The side walls of the waveguides are considered perfectly reflecting.

2.1. Acoustic field in front of wall surface

The sound pressure of a time-harmonic incident plane wave is given by

$$p_{\mathrm{inc}}(x,y,z) = \mathrm{e}^{\mathrm{j}(\alpha_0 x + \beta_0 y + \gamma_0 z)}, \quad \begin{cases} \alpha_0 = k \sin\theta \sin\varphi, \\ \beta_0 = k \cos\theta, \\ \gamma_0 = k \sin\theta \cos\varphi, \end{cases} \tag{3}$$

where k is the wave number and (θ,φ) defines the incidence shown in Fig. 3. The complex time factor of the form $\mathrm{e}^{\mathrm{j}\omega t}$ is omitted.

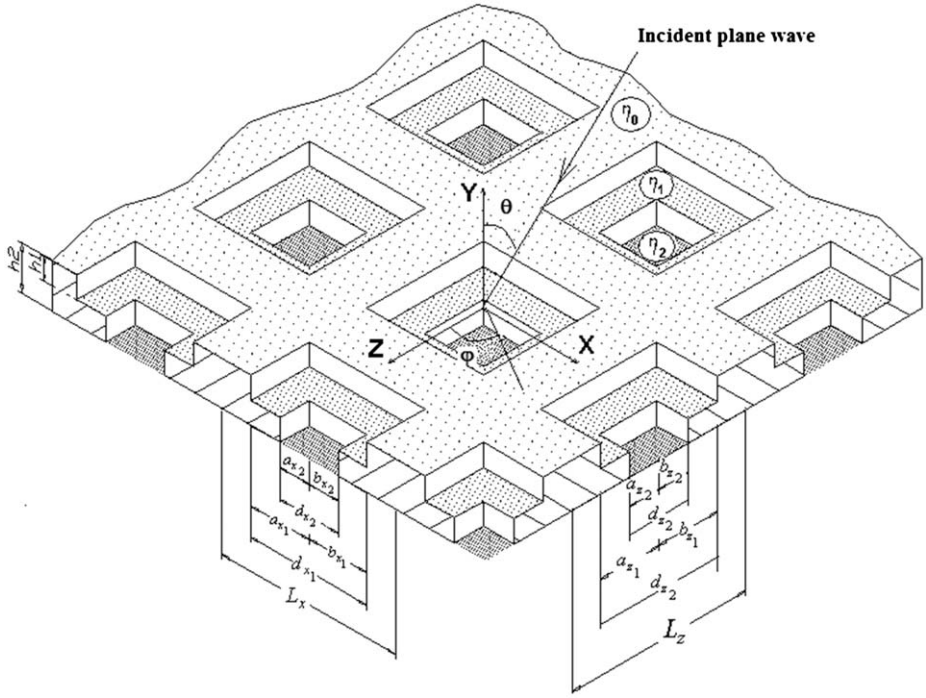

Fig. 4. 2D periodic uneven surface of rectangular profile with two waveguides in the context of profile A.

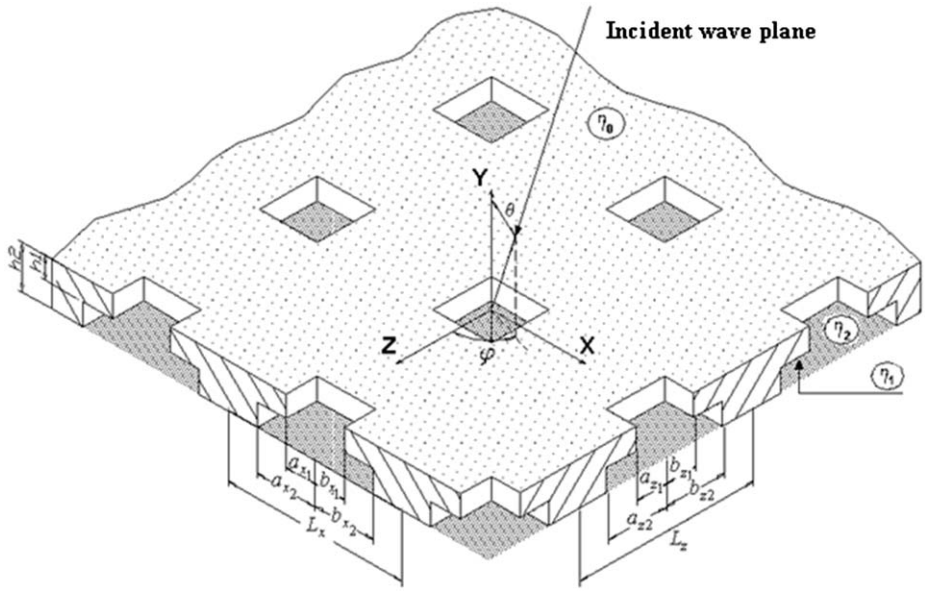

Fig. 5. 2D periodic uneven surface of rectangular profile with two waveguides in the context of profile B.

As in the 1D periodic surface profiles introduced by Ando and Kato [15], the acoustic field in front of the wall (i.e. at $y>0$, corresponding to region I) for the 2D periodic profiles can be expressed as the superposition of the incident and the reflected fields:

$$p_{\mathrm{I}}(x,y,z)=p_{\mathrm{inc}}+p_{\mathrm{ref}}=\mathrm{e}^{\mathrm{j}(\alpha_0 x+\beta_0 y+\gamma_0 z)}+\sum_{r,s=-\infty}^{+\infty}R_{r,s}\mathrm{e}^{\mathrm{j}(\alpha_r x-\beta_{r,s} y+\gamma_s z)}, \tag{4}$$

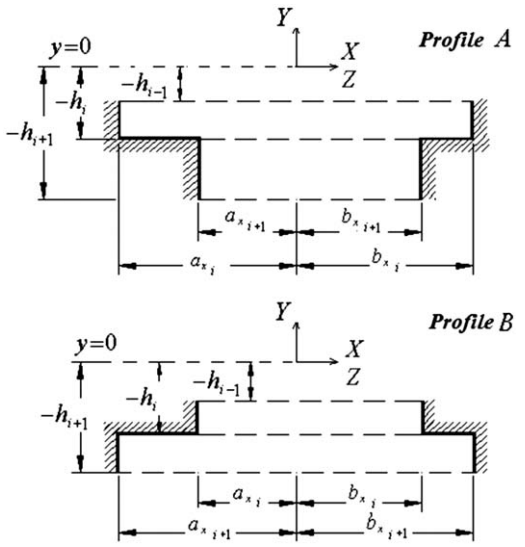

Fig. 6. Profiles A and B with N waveguides.

where

$$\begin{cases} \alpha_r = \alpha_0 + 2\pi r/L_x, \\ \gamma_s = \gamma_0 + 2\pi s/L_z. \end{cases} \tag{5}$$

Eq. (4) shows that the total reflected acoustic pressure is composed of an infinity of plane waves of order $(r,s) = 0, \pm 1, \pm 2, \ldots \pm\infty$. Each mode possesses an amplitude $R_{r,s}$ that must be determined. For (r,s) such as $\alpha_r^2 + \gamma_s^2 \le k^2$, $\beta_{r,s}$ are real and the associated modes propagate in the direction defined by $\theta_{r,s}$ and $\varphi_{r,s}$ such as

$$\begin{cases} \alpha_r = k\sin(\theta_{r,s})\sin(\varphi_{r,s}), \\ \beta_{r,s} = k\cos(\theta_{r,s}), \\ \gamma_s = k\sin(\theta_{r,s})\cos(\varphi_{r,s}). \end{cases} \tag{6}$$

The (r,s) values in the case of $\alpha_r^2 + \gamma_s^2 > k^2$ correspond to non-propagating reflection modes, depending on the sign of $\beta_{r,s}$. The complex amplitudes of these modes decrease or increase exponentially. The sign is chosen such that the amplitude of the considered mode does not tend to infinity. $\beta_{r,s}$ is defined by

$$\begin{cases} \beta_{r,s} = (k^2 - \alpha_r^2 - \gamma_s^2)^{1/2}, & \alpha_r^2 + \gamma_s^2 \le k^2, \\ \beta_{r,s} = -\mathrm{j}(\alpha_r^2 + \gamma_s^2 - k^2)^{1/2}, & \alpha_r^2 + \gamma_s^2 > k^2. \end{cases} \tag{7}$$

Such modes are evanescent in the normal incidence to the wall.

To determine $R_{r,s}$, one has to express the acoustic pressure p_{II} inside the surface cavities (i.e. for $y < 0$, corresponding to region II).

2.2. Formulation

Helmholtz equations above the wall (i.e. for $y > 0$) and associated with the waveguide i are

$$\left(\frac{\partial^2}{\partial x^2} + \frac{\partial^2}{\partial y^2} + \frac{\partial^2}{\partial z^2}\right) p_{\mathrm{I}} + k^2 p_{\mathrm{I}} = 0, \quad y > 0, \forall x, \forall z \tag{8}$$

and

$$\left(\frac{\partial^2}{\partial x^2} + \frac{\partial^2}{\partial y^2} + \frac{\partial^2}{\partial z^2}\right) p_i + k^2 p_i = 0, \quad -h_i < y < -h_{i-1}, \begin{cases} v_x L_x + a_{x_i} < x < v_x L_x + b_{x_i}, \\ v_z L_z + a_{z_i} < z < v_z L_z + b_{z_i}, \end{cases} \tag{9}$$

where p_{I} and p_i are the acoustic pressures in front of the wall (i.e. for $y > 0$) and correspond to the waveguide i, respectively. Each cavity is identified by the couple (v_x, v_z).

Using the coordinates in the mentioned groove

$$x_{v_x} = x - v_x L_x \tag{10}$$

and

$$z_{v_z} = z - v_z L_z. \tag{11}$$

Boundary conditions are

$$\frac{\partial p_i}{\partial x_v} = 0, \quad -h_i < y < -h_{i-1}, a_{z_i} < z_v < b_{z_i}, \ \{x_v = a_{x_i} \text{ or } x_v = b_{x_i}\}, \quad i = 1, 2, \ldots N, \tag{12}$$

$$\frac{\partial p_i}{\partial z_v} = 0, \quad -h_i < y < -h_{i-1}, a_{x_i} < x_v < b_{x_i}, \ \{z_v = a_{z_i} \text{ or } z_v = b_{z_i}\}, \ i = 1, 2, \ldots N, \tag{13}$$

$$\frac{\partial p_1}{\partial y} - \mathrm{j}k\eta_0 p_1 = 0, \quad \begin{cases} -L_x/2 < x_v < a_{x_1}, & b_{x_1} < x_v < L_x/2, \\ -L_z/2 < z_v < a_{z_1}, & b_{z_1} < z_v < L_z/2, \end{cases} \tag{14}$$

$$p_1 = p_1, \quad y = 0, \quad a_{x_1} < x_v < b_{x_1}, \quad a_{z_1} < z_v < b_{z_1}, \tag{15}$$

$$\frac{\partial p_1}{\partial y} = \frac{\partial p_1}{\partial y}, \quad y = 0, \quad a_{x_1} < x_v < b_{x_1}, \quad a_{z_1} < z_v < b_{z_1}, \tag{16}$$

Eqs. (15) and (16) lead to

$$\frac{\partial p_1}{\partial y} - \mathrm{j}k\eta_0 p_1 = \frac{\partial p_1}{\partial y} - \mathrm{j}k\eta_0 p_1, \tag{17}$$

$$\frac{\partial p_N}{\partial y} - \mathrm{j}k\eta_N p_N = 0, \quad y = -h_N, \quad a_{x_N} < x_v < b_{x_N}, \quad a_{z_N} < z_v < b_{z_N}. \tag{18}$$

Sound velocity and pressure continuity conditions between two waveguides can be expressed in two different ways, as a function of the boundary pattern.

- In the case of profile A (Fig. 4), theses conditions are

$$\frac{\partial p_i}{\partial y} - \mathrm{j}k\eta_i p_i = 0, \quad y = -h_i, \quad \begin{cases} a_{x_i} < x_v < a_{x_{i+1}}, & b_{x_{i+1}} < x_v < b_{x_i} \\ a_{z_i} < z_v < a_{z_{i+1}}, & b_{z_{i+1}} < z_v < b_{z_i} \end{cases} \tag{19}$$

$$\frac{\partial p_i}{\partial y} = \frac{\partial p_{i+1}}{\partial y}, \quad y = -h_i, \quad a_{x_{i+1}} < x_v < b_{x_{i+1}}, \quad a_{z_{i+1}} < z_v < b_{z_{i+1}} \tag{20}$$

$$p_i = p_{i+1}, \quad y = -h_i, \quad a_{x_{i+1}} < x_v < b_{x_{i+1}}, \quad a_{z_{i+1}} < z_v < b_{z_{i+1}} \tag{21}$$

- In the case of profile B (Fig. 5), theses conditions are

$$\frac{\partial p_{i+1}}{\partial y} - \mathrm{j}k\eta_i p_{i+1} = 0, \quad y = -h_i, \quad \begin{cases} a_{x_{i+1}} < x_v < a_{x_i}, & b_{x_i} < x_v < b_{x_{i+1}} \\ a_{z_{i+1}} < z_v < a_{z_i}, & b_{z_i} < z_v < b_{z_{i+1}} \end{cases} \tag{22}$$

$$\frac{\partial p_i}{\partial y} = \frac{\partial p_{i+1}}{\partial y}, \quad y = -h_i, \quad a_{x_i} < x_v < b_{x_i}, \quad a_{z_i} < z_v < b_{z_i} \tag{23}$$

$$p_i = p_{i+1}, \quad y = -h_i, \quad a_{x_i} < x_v < b_{x_i}, \quad a_{z_i} < z_v < b_{z_i} \tag{24}$$

2.3. Acoustic field in the surface cavities

The acoustic field in the cavity, identified by the couple (v_x, v_z), is defined as a superposition of waveguide modes along the y-axis:

$$p_i(x_v, z_v) = \mathrm{e}^{\mathrm{j}\alpha_0 v_x L_x} \mathrm{e}^{\mathrm{j}\gamma_0 v_z L_z} \left\{ \sum_{m,n=0}^{+\infty} (A^i_{m,n} \mathrm{e}^{\mathrm{j}\chi^i_{m,n} y} + B^i_{m,n} \mathrm{e}^{-\mathrm{j}\chi^i_{m,n} y}) \psi^{x,i}_m \psi^{z,i}_n \right\} \tag{25}$$

where

$$\begin{cases} \chi^i_{m,n} = (k^2 - m^2\pi^2/d^2_{x_i} - n^2\pi^2/d^2_{z_i})^{1/2}, & m^2\pi^2/d^2_{x_i} + n^2\pi^2/d^2_{z_i} < k^2 \\ \chi^i_{m,n} = -\mathrm{j}(m^2\pi^2/d^2_{x_i} + n^2\pi^2/d^2_{z_i} - k^2)^{1/2}, & m^2\pi^2/d^2_{x_i} + n^2\pi^2/d^2_{z_i} > k^2 \end{cases} \tag{26}$$

with

$$\psi_m^{x,i}(x_v)=\cos\left(\frac{m\pi}{d_{x_i}}(x_v-b_x)\right),\quad \psi_n^{z,i}(z_v)=\cos\left(\frac{n\pi}{d_{z_i}}(z_v-b_z)\right) \tag{27}$$

$\alpha_r, \beta_{r,s}$ and γ_s are defined by Eqs. (5) and (7).

Substituting x by $x_{v_x}=x-v_xL_x$ and z by $z_{v_z}=z-v_zL_z$ in Eq. (4) and inserting the modified Eq. (4), as well as Eq. (26) for i=1, into Eq. (18) leads to

$$(\beta_0-k\eta_0)e^{j\alpha_0x_{v_x}}e^{j\gamma_0z_{v_z}}-\sum_{r,s=-\infty}^{r=+\infty}R_{r,s}(\beta_{r,s}+k\eta_0)e^{j\alpha_rx_{v_x}}e^{j\gamma_sz_{v_z}}=\sum_{m,n=0}^{+\infty}[A_{mn}^1(\chi_{mn}^1-k\eta_0)-(\chi_{mn}^1+k\eta_0)B_{mn}^1]\psi_{mn}(x_{v_x},z_{v_z}) \tag{28}$$

By multiplying each term of Eq. (28) by $e^{-j\alpha_rx_{v_x}}e^{-j\gamma_sz_{v_z}}$ and integrating:

- the left-hand side on x_{v_x} between $-L_x/2$ and $+L_x/2$ and on z_{v_z} between $-L_z/2$ and $+L_z/2$ (it involves the positive y space and the entire surface of a cell of the periodic structure), and
- the right-hand side on x_{v_x} between a_{x_1} and b_{x_1} and on z_{v_z} between a_{z_1} and b_{z_1} (it covers the whole surface of the first waveguide).

It is possible to express the amplitudes $R_{r,s}$ of the reflected waves (Eq. (29)) and those of $A_{s,t}^1$ and $B_{s,t}^1$ in the first waveguide (located near the surface) using the orthogonal properties of exponential functions and Eq. (14):

$$R_{r,s}=\frac{\beta_{0,0}-k\eta_0}{\beta_{0,0}+k\eta_0}\mu_{r,s}-\frac{d_{x_1}d_{z_1}}{L_xL_z}\sum_{m,n=0}^{+\infty}(A_{m,n}^1(\chi_{m,n}^1-k\eta_0)-(\chi_{m,n}^1+k\eta_0)B_{m,n}^1)\frac{u_{m,n,r,s}^*}{\beta_{r,s}+k\eta_0},\quad (r,s)=0\pm1,\pm2\ldots \tag{29}$$

where $\mu_{0,0}$=1 and $\mu_{r,s}$=0 for $(r,s)\neq(0,0)$ and:

$$u_{m,n,r,s}=\frac{1}{d_{x_1}}\int_{a_{x_1}}^{b_{x_1}}\psi_m^{x,1}(x_v)e^{j\alpha_rx_v}\,dx_v\frac{1}{d_{z_1}}\int_{a_{z_1}}^{b_{z_1}}\psi_n^{z,1}(x_v)e^{j\gamma_rz_v}\,dz_v=u_{m,r}^xu_{n,s}^z \tag{30}$$

$$u_{m,r}^x=\frac{-j\alpha_r}{d_{x_1}(\alpha_r^2-m^2\pi^2/d_{x_1}^2)}(e^{j\alpha_rb_{x_1}}-(-1)^me^{j\alpha_ra_{x_1}}) \tag{31}$$

$$u_{n,s}^z=\frac{-j\gamma_s}{d_{z_1}(\gamma_s^2-n^2\pi^2/d_{z_1}^2)}(e^{j\gamma_sb_{z_1}}-(-1)^ne^{j\gamma_sa_{z_1}}) \tag{32}$$

$$A_{s,t}^1+B_{s,t}^1=b_{s,t}-\varepsilon_s\varepsilon_t\frac{d_{x_1}d_{z_1}}{L_xL_z}\sum_{m,n=0}^{+\infty}\{(A_{m,n}^1(\chi_{m,n}^1-k\eta_0)-B_{m,n}^1(\chi_{m,n}^1+k\eta_0))V_{m,n,s,t}\},\quad (s,t)=0,1,2\ldots, \tag{33}$$

where

$$V_{m,n,s,t}=\sum_{r,p=-\infty}^{+\infty}\frac{u_{m,n,r,p}^*u_{s,t,r,p}}{\beta_{r,p}+k\eta_0},\quad b_{s,t}=\varepsilon_s\varepsilon_t\frac{2\beta_0u_{s,t,0,0}}{\beta_0+k\eta_0} \tag{34}$$

where ε_0=1, ε_s=2 if $s\neq0$, and the asterisk indicates the complex conjugate.

The amplitude $R_{r,s}$ can be determined with Eq. (30) providing we know $A_{m,n}^1$ and $B_{m,n}^1$.

The boundary conditions of the bottom interstice (Eq. (18)) and the expression for sound pressure at i=N (Eq. (25)), results in

$$B_{m,n}^N=A_{m,n}^N\frac{\chi_{m,n}^N-k\eta_N}{\chi_{m,n}^N+k\eta_N}e^{-2j\chi_{m,n}^Nh_N}=A_{m,n}^N\Gamma_{m,n}^N \tag{35}$$

The continuity conditions of velocities between two waveguides (Eq. (20) or (23) depending on the profile type) and the sound pressure expression for the waveguide i (Eq. (25)) yield for the two different profiles A and B, respectively:

$$(\chi_{s,t}^i-k\eta_i)A_{s,t}^ie^{-j\chi_{s,t}^ih_i}-(\chi_{s,t}^i+k\eta_i)B_{s,t}^ie^{j\chi_{s,t}^ih_i}=\frac{\varepsilon_s\varepsilon_t}{d_{x_i}d_{z_i}}\sum_{m,n=0}^{+\infty}[(\chi_{m,n}^{i+1}-k\eta_i)A_{m,n}^{i+1}e^{-j\chi_{m,n}^{i+1}h_i}-(\chi_{m,n}^{i+1}+k\eta_i)B_{m,n}^{i+1}e^{j\chi_{m,n}^{i+1}h_i}]v_{m,n,s,t,i} \tag{36}$$

where

$$v_{m,s,n,t,i}=\int_{a_{x_{i+1}}}^{b_{x_{i+1}}}\psi_m^{x,i+1}(x_v)\psi_s^{x,i}(x_v)\,dx_v\int_{a_{z_{i+1}}}^{b_{z_{i+1}}}\psi_n^{z,i+1}(z_v)\psi_t^{z,i}(z_v)\,dz_v \tag{37}$$

$$(\chi_s^{i+1}+k\eta_i)A_s^{i+1}e^{-j\chi_s^{i+1}h_i}-(\chi_s^{i+1}-k\eta_i)B_s^{i+1}e^{j\chi_s^{i+1}h_i}=\frac{\varepsilon_s}{d_{x_{i+1}}}\sum_{m=0}^{+\infty}[(\chi_m^i+k\eta_i)A_m^ie^{-j\chi_m^ih_i}-(\chi_m^i-k\eta_i)B_m^ie^{j\chi_m^ih_i}]w_{m,s,i} \tag{38}$$

where

$$w_{m,s,n,t,i} = \int_{a_{x_i}}^{b_{x_i}} \psi_m^{x,i}(x_v)\psi_s^{x,i+1}(x_v)\,\mathrm{d}x_v \int_{a_{z_i}}^{b_{z_i}} \psi_n^{z,i}(z_v)\psi_t^{z,i+1}(z_v)\,\mathrm{d}z_v \tag{39}$$

An identical argument about the sound pressure continuity condition of Eq. (21) (or Eq. (24)) provides, for the profiles A and B:

$$A_{s,t}^{i+1}\mathrm{e}^{-\mathrm{j}\chi_{s,t}^{i+1}h_i} + B_{s,t}^{i+1}\mathrm{e}^{\mathrm{j}\chi_{s,t}^{i+1}h_i} = \frac{\varepsilon_s\varepsilon_t}{d_{x_{i+1}}d_{z_{i+1}}} \sum_{m,n=0}^{+\infty} (A_{m,n}^{i}\mathrm{e}^{-\mathrm{j}\chi_{m,n}^{i}h_i} + B_{m,n}^{i}\mathrm{e}^{\mathrm{j}\chi_{m,n}^{i}h_i})\nu_{s,t,m,n,i} \tag{40}$$

$$A_{s,t}^{i}\mathrm{e}^{-\mathrm{j}\chi_{s,t}^{i}h_i} + B_{s,t}^{i}\mathrm{e}^{\mathrm{j}\chi_{s,t}^{i}h_i} = \frac{\varepsilon_s\varepsilon_t}{d_{x_i}d_{z_i}} \sum_{m,n=0}^{+\infty} (A_{m,n}^{i+1}\mathrm{e}^{-\mathrm{j}\chi_{m,n}^{i+1}h_i} + B_{m,n}^{i+1}\mathrm{e}^{\mathrm{j}\chi_{m,n}^{i+1}h_i})w_{s,t,m,n,i}. \tag{41}$$

Eqs. (36) and (40), (or Eqs. (38) and (41), depending on the geometry of the two waveguides), Eqs. (31), (33) and (35) generate a system of $2N+1$ equations with $2N+1$ variables. The unknowns of this system are the amplitudes of the incident waveguides $A_{m,n}^{i}$ $(i=1,2,\ldots,N,\ (m,n)=0,1,\ldots,+\infty)$, the amplitude of the reflected waveguides $B_{m,n}^{i}$ $(i=1,2,\ldots,N\sqrt{2},\ (m,n)=0,1,\ldots,+\infty)$ in each waveguide, and the amplitude of the reflected waves above the wall $R_{r,s}$ $((r,s)=0\pm1,\pm2,\ldots,\pm\infty)$.

The amplitude $R_{r,s}$ can be determined with the equation systems Eqs. (29) and (33) providing that we can express the unknowns $B_{s,t}^{1}$ $((s,t)=0,1,\ldots,+\infty)$ as functions of $A_{s,t}^{1}$ $((s,t)=0,1,\ldots,+\infty)$. These amplitudes are, respectively, the amplitude of the incident and the first reflected waveguide.

The problem is now to find a relationship in form of $\mathbf{B}^1=f(\mathbf{A}^1)$, where $\mathbf{A}^1$ and $\mathbf{B}^1$ are vectors with the amplitudes $A_{s,t}^{1}$ $((s,t)=0,1,\ldots,+\infty)$ and $B_{s,t}^{1}$ $((s,t)=0,1,\ldots,+\infty)$, respectively, as coordinates.

The same argument as that elaborated for the 1D periodic profile is used here. It is an iterative method that involves determining a relationship in the form of $\mathbf{B}^i=f(\mathbf{A}^i)$, for $i=N,N-1,\ldots,1$ for each waveguide, starting from the bottom to the top.

The relationship $\mathbf{B}^N=f(\mathbf{A}^N)$ is directly given by Eq. (35). This expression shows the absence of a coupling between various modes in the last waveguide. It is possible to express Eq. (35) in the following way:

$$B_{m,n}^{N} = A_{m,n}^{N}\Gamma_{m,n}^{N} = \sum_{(s,t)=0}^{+\infty} \Gamma_{m,n,s,t}^{N}A_{s,t}^{N} \tag{42}$$

where

$$\Gamma_{m,n,s,t}^{N} = \Gamma_{m,n}^{N} \quad \text{if } m=s \quad \text{and} \quad n=t \quad \text{else } \Gamma_{m,n,s,t}^{N}=0 \tag{43}$$

By replacing i by $N-1$ in Eq. (36) and (40) (or Eq. (38) and (41) as the geometry of the waveguides N and $N-1$ corresponds to a profile A or B), then by replacing the unknowns $B_{m,n}^{N}$ in these two equations as expressed by Eq. (42), it follows:

for a profile A:

$$\begin{aligned}&(\chi_{n,p}^{N-1}-k\eta_{N-1})\mathrm{e}^{-\mathrm{j}\chi_{n,p}^{N-1}h_{N-1}}A_{n,p}^{N-1} - (\chi_{n,p}^{N-1}+k\eta_{N-1})\mathrm{e}^{\mathrm{j}\chi_{n,p}^{N-1}h_{N-1}}B_{n,p}^{N-1}\\ &\quad= \frac{\varepsilon_n\varepsilon_p}{d_{x_{N-1}}d_{z_{N-1}}} \sum_{(t,x)=0}^{+\infty}\left[\sum_{(m,s)=0}^{+\infty}[(\chi_{m,s}^{N}-k\eta_{N-1})\delta_{m,t}\delta_{s,x}\mathrm{e}^{-\mathrm{j}\chi_{m,s}^{N}h_{N-1}} - (\chi_{m,s}^{N}+k\eta_{N-1})\Gamma_{m,t,s,x}^{N}\mathrm{e}^{\mathrm{j}\chi_{m,s}^{N}h_{N-1}}]\nu_{m,n,s,p,N-1}\right]A_{t,x}^{N}, \quad (n,p)=0,1,2,\ldots\end{aligned} \tag{44}$$

where $\delta_{m,n}$ is the Kronecker delta function, i.e. $\delta_{m,n}=0$ if $n\neq m$ and $\delta_{m,n}=1$ if $n=m$, and

$$\sum_{(t,x)=0}^{+\infty}(\delta_{n,t}\delta_{p,x}+\Gamma_{n,t,p,x}^{N}\mathrm{e}^{2\mathrm{j}\chi_{n,p}^{N}h_{N-1}})A_{t,x}^{N} = \frac{\varepsilon_n\varepsilon_p\mathrm{e}^{\mathrm{j}\chi_{n,p}^{N}h_{N-1}}}{d_{x_N}d_{z_N}} \sum_{(m,s)=0}^{+\infty}(A_{m,s}^{N-1}\mathrm{e}^{-\mathrm{j}\chi_{m,s}^{N-1}h_{N-1}} + B_{m,s}^{N-1}\mathrm{e}^{\mathrm{j}\chi_{m,s}^{N-1}h_{N-1}})\nu_{n,m,p,s,N-1}, \quad (n,p)=0,1,2,\ldots \tag{45}$$

for a profile B:

$$\begin{aligned}&\sum_{(t,x)=0}^{+\infty}\left[\delta_{n,t}\delta_{p,x} - \frac{(\chi_{n,p}^{N}-k\eta_{N-1})}{(\chi_{n,p}^{N}+k\eta_{N-1})}\Gamma_{n,t,p,x}^{N}\mathrm{e}^{2\mathrm{j}\chi_{n,p}^{N}h_{N-1}}\right]A_{t,x}^{N}\\ &\quad= \frac{\varepsilon_n\varepsilon_p}{d_{x_N}d_{z_N}}\frac{\mathrm{e}^{\mathrm{j}\chi_{n,p}^{N}h_{N-1}}}{(\chi_{n,p}^{N}+k\eta_{N-1})} \sum_{(m,s)=0}^{+\infty}[(\chi_{m,s}^{N-1}+k\eta_{N-1})A_{m,s}^{N-1}\mathrm{e}^{-\mathrm{j}\chi_{m,s}^{N-1}h_{N-1}} - (\chi_{m,s}^{N-1}-k\eta_{N-1})B_{m,s}^{N-1}\mathrm{e}^{\mathrm{j}\chi_{m,s}^{N-1}h_{N-1}}]w_{m,n,s,p,N-1}, \quad (n,p)=0,1,2,\ldots\end{aligned} \tag{46}$$

and

$$A_{n,p}^{N-1}\mathrm{e}^{-\mathrm{j}\chi_{n,p}^{N-1}h_{N-1}} + B_{n,p}^{N-1}\mathrm{e}^{\mathrm{j}\chi_{n,p}^{N-1}h_{N-1}} = \frac{\varepsilon_n\varepsilon_p}{\mathrm{d}_{x_{N-1}}\mathrm{d}_{z_{N-1}}} \sum_{(t,x)=0}^{+\infty}[\sum_{(m,s)=0}^{+\infty}(\delta_{t,m}\delta_{x,s}\mathrm{e}^{-\mathrm{j}\chi_{m,s}^{N}h_{N-1}} + \Gamma_{t,m,x,s}^{N}\mathrm{e}^{\mathrm{j}\chi_{m,s}^{N}h_{N-1}})w_{n,m,p,s,N-1}]A_{t,x}^{N}, \quad (n,p)=0,1,2,\ldots \tag{47}$$

Inversion of the system given by Eq. (45) allows us to eliminate the unknown $A^N_{t,x}$ from Eqs. (44) and (47) and to obtain, in the case of profile A, a relationship in the form of $\mathbf{B}^{N-1}=\mathbf{\Gamma}^{N-1}\otimes\mathbf{A}^{N-1}$, where $\otimes$ is the matrix product. This relationship can be also obtained for a profile B by inverting the equation system Eq. (46).

By iterating the previous process for each of the waveguides, we can obtain numerically the relation $\mathbf{B}^1=\mathbf{\Gamma}^1\otimes\mathbf{A}^1$ in the first waveguide.

Insertion of this relation in Eq. (29) leads to:

$$R_{r,s}=\frac{\beta_{0,0}-k\eta_0}{\beta_{0,0}+k\eta_0}\mu_{r,s}-\frac{d_{x_1}d_{z_1}}{L_xL_z}\sum_{(t,p)=0}^{+\infty}\left[\sum_{(m,n)=0}^{+\infty}(\delta_{m,t}\delta_{n,p}(\chi^1_{m,n}-k\eta_0)-\Gamma^1_{m,t,n,p}(\chi^1_{m,n}+k\eta_0))\frac{u^*_{m,r}}{\beta_{r,s}+k\eta_0}\right]A^1_{t,p},\quad (r,s)=0\pm1,\pm2,\ldots \tag{48}$$

Also, the transfer of Γ^1 in Eq. (33) yields:

$$\sum_{(t,s)=0}^{+\infty}W_{n,p,t,s}A^1_{t,s}=b_{n,p},\quad (n,p)=0,1,2\ldots \tag{49}$$

with

$$W_{n,p,t,s}=(\delta_{n,t}\delta_{p,s}+\Gamma^1_{n,t,p,s})+\varepsilon_n\varepsilon_p\frac{d_{x_1}d_{z_1}}{L_xL_z}$$

$$\sum_{(m,x)=0}^{+\infty}(\delta_{t,m}\delta_{s,x}(\chi^1_{m,x}-k\eta_0)-\Gamma^1_{t,m,s,x}(\chi^1_{m,x}+k\eta_0))V_{m,n,x,s},\quad (n,p,t,s)=0,1,2,\ldots \tag{50}$$

where $V_{m,n,x,s}$ and $b_{n,p}$ are defined in Eq. (34).

And finally, the numerical resolution of the system given by Eq. (49)[1] for the amplitudes $A^1_{t,s}$ $((t,s)=0,1,2,\ldots)$ of the first waveguide and the insertion of these solutions into Eq. (48) provide the amplitudes $R_{r,s}$ of the waves reflected by the wall.

3. Experimental validation

Measurements have been carried out in free-field conditions in the INRS (French national research institute for occupational health and safety) semi-anechoic chamber. 2D periodic surfaces with one and two waveguides were used to validate the waveguide model developed in Section 2. These profiles are made of polystyrene blocks with a high acoustic reflection coefficient (see Fig. 9). This coefficient was measured using a two-microphone technique [18] to deduce the specific acoustic admittance η_0 required in the waveguide model. The reflection measurement is error sensitive, when the studied facing is highly reflective. The curve representing this coefficient appeared relatively noisy. We therefore chose a constant specific acoustic admittance η_0=0.08, which gave an acoustic reflection coefficient of approximately 0.85–0.9 (see Fig. 9). The specific acoustic admittance η_0 is defined as the ratio of the characteristic acoustic impedance of air $\rho_0 c$ to the characteristic acoustic impedance of polystyrene $\rho_p c_p$ [19]:

$$\eta_0=\frac{\rho c}{\rho_p c_p}=\frac{1.2\times344}{12\times430}=0.08 \tag{51}$$

The waveguide model provides solutions to problems of sound reflection on periodic wall profiles, when the incident sound field is made up of plane waves of differing incidence. In practice, plane waves are very difficult to generate. A conventional sound source can therefore be used and the waveguide model adapted to the source intensity distribution.

The chosen source was a 10 cm diameter Pioneer TS E1077 loudspeaker. This was connected to a B&K 1405 noise generator through a Power APK 2000 amplifier and a Yamaha GQ 1031 Graphic Equaliser to generate pink noise. B&K 4935 1/4″ microphones were used for acquisition, connected to a B&K 2694 Deltatron conditioner. The acquisition system was an OROS OR25. Signal acquisition was performed at a 25 600 Hz sampling frequency for 30 s. Digital simulations were nevertheless restricted to a lower range (3000 Hz). Computation times would have been too long beyond this frequency.

3.1. Sound source

The loudspeaker was considered a dipolar source weighted by a directivity factor. The source position was defined by its radial vector $\mathbf{r}_s$ and its coordinates x_s, y_s and z_s as shown in Fig. 7. The incident sound field emitted by the source at the sensor position defined by the radial vector $\mathbf{r}_c$ and by coordinates x_c, y_c and z_c can be expressed as [17]

$$p_{\mathrm{inc}}(\mathbf{r}_c,\mathbf{r}_s)=\cos(\theta)\left(1+\frac{1}{\mathrm{j}k|\mathbf{r}_c-\mathbf{r}_s|}\right)\frac{\mathrm{e}^{-\mathrm{j}k|\mathrm{r}_c-\mathrm{r}_s|}}{|\mathbf{r}_c-\mathbf{r}_s|}=\frac{y_s-y_c}{|\mathbf{r}_c-\mathbf{r}_s|}\left(1+\frac{1}{\mathrm{j}k|\mathbf{r}_c-\mathbf{r}_s|}\right)\frac{\mathrm{e}^{-\mathrm{j}k|\mathrm{r}_c-\mathrm{r}_s|}}{|\mathbf{r}_c-\mathbf{r}_s|} \tag{52}$$

[1] This resolution needs the truncation of infinite systems. This operation is achieved by comparing two simulations of the same problem processed for two different orders of truncation and by verifying that the results are identical. In this case, we are sure that the first solutions converge.

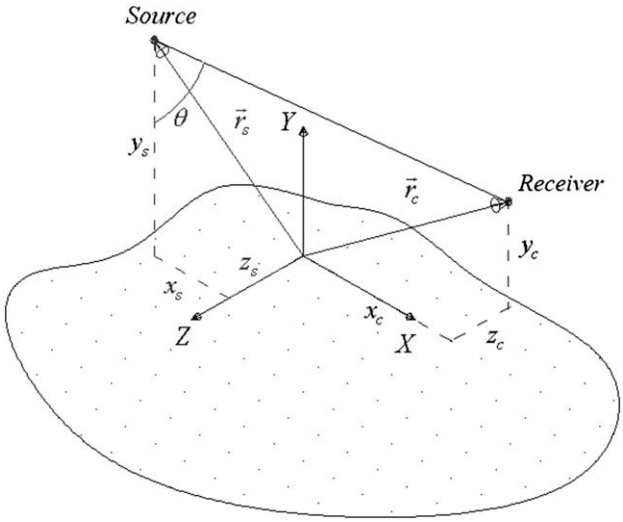

Fig. 7. System of coordinates used to describe the source and the sensors positions.

The angular distribution of the directivity factor ($\cos(\theta)$) can be represented by means of the amplitude of the incident sound pressure using the following spatial Fourier transform:

$$\tilde{p}_{\mathrm{inc}}(\alpha_0) = \int_{-\infty}^{+\infty} p_{\mathrm{inc}}(x) \mathrm{e}^{\mathrm{j}\alpha_0 x_c}\, \mathrm{d}x_c \tag{53}$$

Eq. (52) was numerically calculated using a Fast Fourier Transform algorithm, which sampled the incident sound field on sensor positions of a sensor array [20]. Fig. 8a illustrates this technique for an array of 45 sensors spaced at d_x=5.5 cm intervals with the central sensor placed at 90 cm right beneath the source.

Transforming the incident field into the wave number domain gives the following angular representation:

$$\alpha_0 = k \sin\theta, \quad \alpha_0 \in [-k, k] \tag{54}$$

Eq. (54) shows that α_0 is the incident wave number projected on sensor lines. The values of α_0 at $|\alpha_0| > k$ correspond to evanescent waves with exponentially decreasing amplitudes. Fig. 8b illustrates the angular distribution of the incident sound field for Fig. 8a configuration.

3.2. Principle of decomposition of the incident sound field

The waveguide model allows us to determine the acoustic pressure reflected in front of periodically uneven wall facings excited by an incident plane wave. Under experimental conditions, the field created by the loudspeaker at $y = 0$ is decomposed into plane waves:

$$p_{\mathrm{inc}}(x, y = 0, z) = \frac{1}{(2\pi)^2} \int\int \tilde{p}_{\mathrm{inc}}(\alpha_0, \gamma_0, y = 0) \mathrm{e}^{-\mathrm{j}(\alpha_0 x + \gamma_0 z)}\, \mathrm{d}\alpha_0\, \mathrm{d}\gamma_0, \tag{55}$$

where the plane wave amplitudes $\tilde{p}_{\mathrm{inc}}$ are determined using the two-dimensional spatial Fourier transform of the incident sound field at $y = 0$:

$$\tilde{p}_{\mathrm{inc}}(\alpha_0, \gamma_0, 0) = \int\int p_{\mathrm{inc}}(x, y = 0, z) \mathrm{e}^{\mathrm{j}(\alpha_0 x + \gamma_0 z)}\, \mathrm{d}x\, \mathrm{d}z. \tag{56}$$

$\tilde{p}_{\mathrm{inc}}$ is numerically determined using a Fast Fourier Transform algorithm. In the case of a 2D periodic profile, spatial samplings Δx and Δz and number of FFT samples n_x and n_z must satisfy the following criteria:

- Spatial samplings must satisfy the Shannon theorem [21]:

$$\Delta x < \frac{c}{2f}, \quad \Delta z < \frac{c}{2f} \tag{57}$$

- Spatial samplings must satisfy:

$$\exists (n_1, n_2) \in \mathbb{N}^2 : \frac{L_x}{\Delta x} = 2^{n_1}, \quad \frac{L_z}{\Delta z} = 2^{n_2} \tag{58}$$

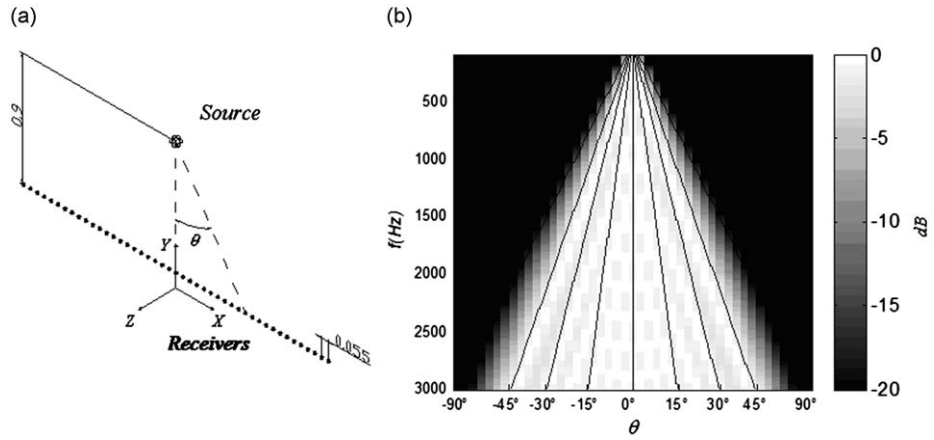

Fig. 8. (a) Schematic of the acoustic pressure measurement using 45 sensors and (b) incident acoustic field decomposition by wave number.

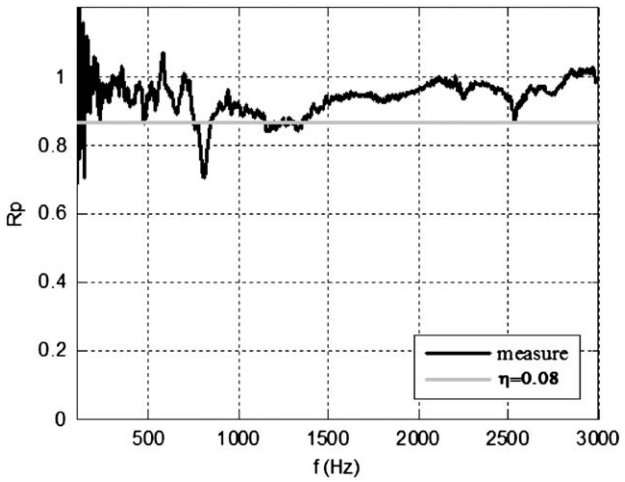

Fig. 9. Acoustic reflection coefficient of polystyrene sample.

Periods L_x and L_z of the 2D periodic profile are both multiples of spatial samplings Δx and Δz. Hence, plane wave incidence angles resulting from sound field decomposition will correspond to the reflected wave characteristic directions (defined by Eq. (5) in Section 2.1).

- Dimensions $L^x_{\text{dec}} = n_x \Delta x$ and $L^z_{\text{dec}} = n_z \Delta z$ of the measurement grid must be large enough for the incident sound field outside the grid range to be considered insignificant.
- The number of FFT samples n_x and n_z must be squares for the FFT algorithm to give acceptable results.

Δx, Δz, n_x and n_z have been chosen based on the following criteria:

$$\Delta x_1 = \frac{c}{2.1f}, \quad \Delta z_1 = \frac{c}{2.1f} \tag{59}$$

where the factor 2.1 has been chosen to assure that the spatial samplings satisfy the Shannon theorem (Eq. (57)) and also to avoid the spatial resolution be too narrow leading to a large number of data requiring long computation times

$$\Delta x = \frac{L_x}{2^{\text{Int}^+(\log_2(\text{Int}^+(L_x/\Delta x_1)))}}, \quad \Delta z = \frac{L_x}{2^{\text{Int}^+(\log_2(\text{Int}^+(L_z/\Delta z_1)))}} \tag{60}$$

$$L^x_{\text{dec}} = L^z_{\text{dec}} = 100\,\text{m} \tag{61}$$

$$n^x_p = 2^{\text{Int}^+(\log_2(L^x_{\text{dec}}/\Delta x))}, \quad n^z_p = 2^{\text{Int}^+(\log_2(L^z_{\text{dec}}/\Delta z))} \tag{62}$$

where $\text{Int}^+(\text{var}) = \text{Int}(\text{var}) + 1$, Int(var) being the integer part of the decimal number var.

For the 1D periodic profile, spatial sampling must satisfy Eq. (58) conditions for the x-axis. In this case, the sampling interval Δz and the FFT sample number n_z along the z-axis are Δx and n_z respectively.

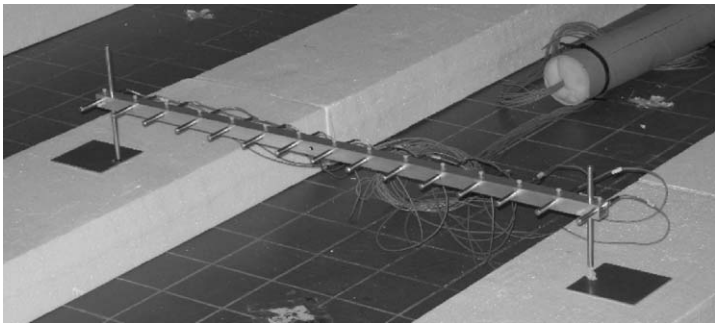

Fig. 10. Array of 15 microphones used to measure the acoustic pressure above the periodic profile.

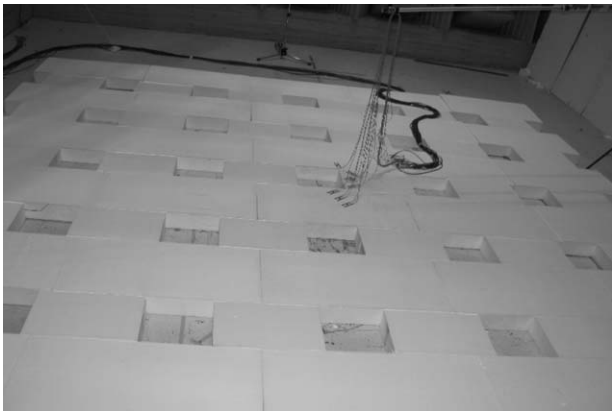

Fig. 11. The investigated 2D periodic profile with one waveguide.

The waveguide model has been applied for each plane wave $\tilde{p}_{\mathrm{inc}}$ produced using the FFT. The total sound field reflected by the periodic profile is then obtained by superposing the elementary reflected sound field calculated for each incident plane wave.

Measurement has been carried out with an array of 15 microphones as shown in Fig. 10. Microphones were spaced at 5.5 cm intervals. The acoustic pressure was measured by 45 sensors as shown in Fig. 8a. Fig. 8b shows the angular distribution of the incidental sound field normalised for every frequency with respect to its maximum value. Array-based measurements were taken three times at three adjacent positions. These positions were chosen such that the central microphone of the 45-sensor virtual array was located directly below the loudspeaker [22].

3.3. Waveguide model validation

3.3.1. 2D periodic profile with one waveguide

In this measurement, x_s, y_s and z_s represent the source and x_c, y_c and z_c, the sensor coordinates, respectively. These dimensions and those of the profiles are expressed in metres.

Fig. 11 illustrates the studied 2D periodic profile with one waveguide. Fig. 12 shows the dimensions of this profile and the admittance values based on the Fig. 3 notations. Fig. 12 also shows the theoretical and the experimental variation of the acoustic pressure at four frequencies (230, 530, 820 and 2275 Hz) for x-coordinates in front of the studied periodic surface. Each acoustic pressure profile is normalised with respect to 1 at the centre of the array and displayed against a linear scale. The loudspeaker is located 1.2 m above the studied surface and the array at 10 cm above. The loudspeaker and the array are centred above the profile at $x=z=0$.

The results obtained from the waveguide method are similar to those obtained through measurement, i.e. the relative mean square errors defined as:

$$E\{(\mathrm{Theoretical}-\mathrm{Experimental})^2\}/E\{\mathrm{Experimental}^2\} \tag{63}$$

where E indicates the expected value, are 0.5, 3.6, 1.7 and 7.4 percent for 230, 530, 820 and 2275 Hz, respectively.

The variation of the acoustic pressure is fairly symmetrical with respect to the centre of the loudspeaker.

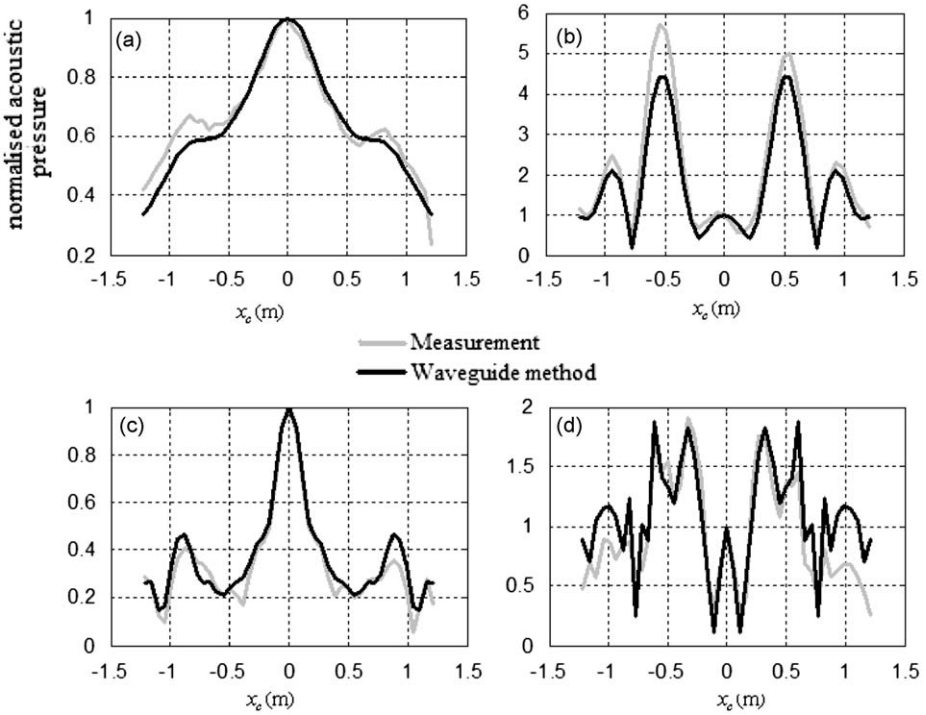

Fig. 12. Acoustic pressure above the studied 2D periodic profile with one waveguide: z_s=0, y_s=1.2, $x_s=\{-1.21,-1.21+0.055,\ldots,1.21\}$, y_c=0.1, z_c=0, L_x=L_z=0.82, d_x=d_z=0.32, h=0.1, η_0=0.08, η_1=0. (a) 230 Hz; (b) 530 Hz; (c) 820 Hz; and (d) 2275 Hz.

Fig. 13. The studied 2D periodic profile with two waveguides—Profile A.

3.3.2. 2D periodic profile with two waveguides—Profile A

x_s, y_s and z_s always represent the coordinates of the source, and x_c, y_c and z_c, those of the sensors. These dimensions as well as those of the profiles are expressed in metres.

The studied 2D periodic profile with two waveguides corresponds to profile A (Fig. 13) which comprises five periods along the x- and z-axes. Fig. 14 shows the dimensions of this profile and the admittance values in metres based on the Fig. 4 notations. Each acoustic pressure profile is normalised with respect to 1 at the centre of the array and shown against a linear scale. The loudspeaker is 1.1 m above the studied surface and the array is 10 cm above. The loudspeaker and array are centred at x=z=0.

Results obtained from the waveguide method are again similar to the measurements despite certain differences at high frequencies. The relative mean square errors are respectively, 0.6, 10.7, 37.5 and 40.8 percent for 230, 530, 820 and 2275 Hz.

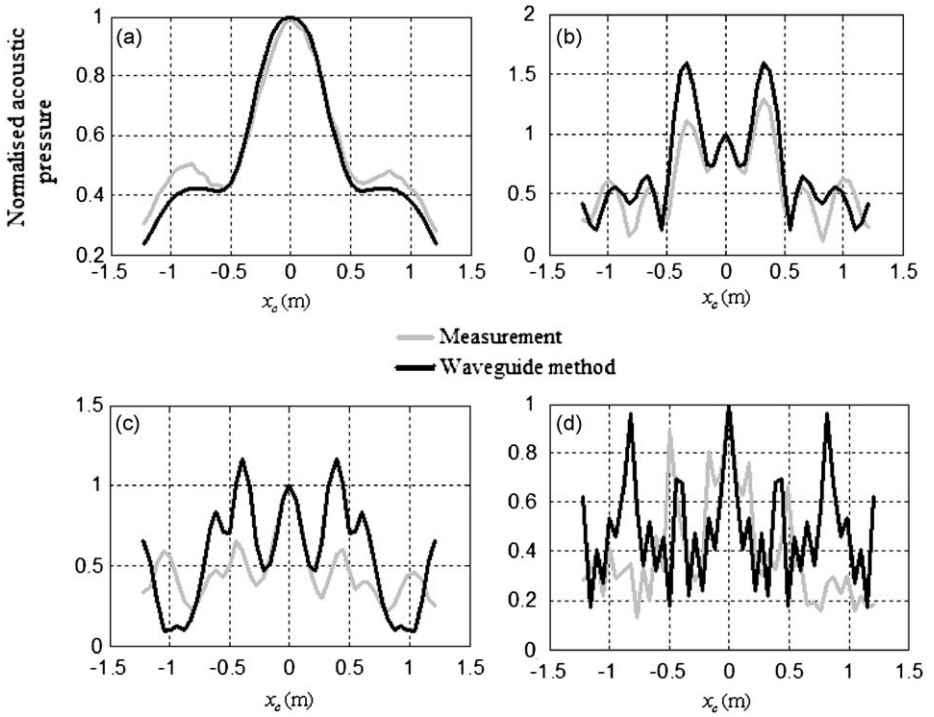

Fig. 14. Acoustic pressure above the studied 2D periodic profile with two waveguides—Profile A: z_s=0, y_s=1.1, $x_s=\{-1.21,-1.21+0.055,\ldots,1.21\}$, y_c=0.1, z_c=0, L_x=L_z=0.82, d_{x1}=d_{z1}=0.57, d_{x2}=d_{z2}=0.32, h_1=h_2=0.1, η_0=η_1=0.08, η_2=0. (a) 230 Hz; (b) 530 Hz; (c) 820 Hz; and (d) 2275 Hz.

Symmetry alone may be considered a validation criterion for both methods. In low frequencies, the close match between the model and experimental results further illustrate the validity of the waveguide model. But it is very difficult to build periodic profiles in a precise way using blocks of polystyrene, particularly profiles with two waveguides. As a result, the measurements become very sensitive to errors at high frequencies because the echoes are very directive and the slightest lack of precision in the positioning of the blocks, of the microphones or of the source can modify considerably the directions and the amplitudes of the reflected waves at the reception points.

3.3.3. *Discussion*

- For the calculation of the acoustic pressure above the studied 2D periodic profile, we chose a constant specific acoustic admittance η_0=0.08, which gave an acoustic reflection coefficient of approximately 0.85–0.9 (see Fig. 9). The experimental result on the profile does appear to suggest that the approximation is acceptable especially at the lower frequencies.
- Measurements at greater distances from the surface have not been carried out because the waveguide method is conceived for infinite surfaces. To avoid the acoustic boundary phenomena of the finite dimensions of the studied profiles, we placed the source (considered as spherical) close to the profile. In these conditions, it would be difficult to place the microphone at greater distances from the surface.

4. Conclusion

When a periodic profile is excited by a plane wave, the reflected sound field can be regarded as superposition of plane waves at specific directions. Periodic uneven surfaces scatter the sound along these directions. The angles of reflection depend on the characteristics of the incident wave and the periodicity of the profile and not on its geometry nor on the acoustic characteristics of the surface itself. Only the amplitudes of the reflected plane waves depend on the geometry and the acoustic properties of the material. These amplitudes are generally difficult to determine. The waveguide method is particularly well adapted to the geometries of periodic profiles encountered in the workshops. This method consists of a spatial sampling of the periodic profile in numerous parallelepipeds. The sound field in each region is defined as the superposition of transverse eigenmodes.

The method of the waveguides has been generalised in this paper to 2D periodic profile composed of rectangular cavities. Measurements have been carried out to validate the waveguide model. The sound source used during the measurements was a loudspeaker located near the studied profile. The waveguide model has been adapted to the case of an incident sound field created by a point source. The simulation results are fairly similar to the experimental ones. Finally, the waveguide method should allow the study of acoustic scattering behaviour to predict the apparent acoustic absorption of periodic profiles observed in acoustic fields in closed spaces.

References

[1] J.W. Rayleigh, *The Theory of Sound*, vol. 2, Dover, New York, 1945 pp. 89–96.
[2] R. Petit, M. Cadillac, Sur la diffraction d'une onde plane par un réseau infiniment conducteur (Diffraction of a plane wave by an infinitely conductive uneven surface), *Comptes Rendus de l'Académie des Sciences, Paris, Ser. B* 262 (1966) 468–471.
[3] A. Purcell, Reflection coefficients for scattering from a pressure-release, sinusoidal surface, *Journal of the Acoustical Society of America* 100 (5) (1996) 2919–2936.
[4] A. Purcell, The Rayleigh equations for a multi-sinusoidal periodic surface, *Journal of the Acoustical Society of America* 103 (2) (1998) 683–694.
[5] R.L. Holford, Scattering of sound waves at a periodic, pressure-release surface: an exact solution, *Journal of the Acoustical Society of America* 70 (14) (1981) 1116–1128.
[6] D. Takahashi, Excess sound absorption due to periodically arranged absorptive materials, *Journal of the Acoustical Society of America* 86 (6) (1989) 2215–2222.
[7] I.A. Urusovskii, Diffraction of sound on a periodically uneven and inhomogeneous surface, *Soviet Physics Acoustics* 5 (1960) 345–348.
[8] J.-J. Embrechts, L. De Geetere, G. Vermeir, M. Vorlander, T. Sakuma, Calculation of the random-incidence scattering coefficients of a sine-shaped surface, *Acta Acustica United With Acustica* 92 (4) (2006) 593–603.
[9] T. Fujimoto, K. Fujiwara, Analysis of sound absorption by periodic structures using a hybrid-boundary element/mode expansion method, *Applied Acoustics* 64 (2003) 525–532.
[10] Y.M. Lam, A boundary integral formulation for the prediction of acoustic scattering from periodic structures, *Journal of the Acoustical Society of America* 105 (2) (1999) 762–769.
[11] P.J. Frey, P.L. George, *Maillage, Application Aux Eléments Finis (Sampling, Application for Finite Element Method)*, Hermes, Paris, 1999.
[12] P. Macey, Acoustic and Structure Interaction Problems Using Finite and Boundary Elements, Ph.D. Thesis, Nottingham University, 1987.
[13] L.N. Deryugin, Equations for the coefficients of wave reflections from a periodically uneven surface, *Doklady Akademii Nauk SSSR* 87 (1952) 913–916.
[14] A. De Bruijn, The sound absorption of an absorbing periodically uneven surface of rectangular profile, *Acustica* 18 (1967) 123–131.
[15] Y. Ando, K. Kato, Calculations on the sound reflection from periodically uneven surfaces of arbitrary profile, *Acustica* 35 (1976) 322–329.
[17] M. Bruneau, *Manuel D'acoustique Fondamentale (Fundamental Acoustics)*, Hermes, Paris, 1998.
[18] J.F. Allard, *Propagation of Sound in Porous Media*, Elsevier Applied Science, London, 1993.
[19] Y. Couasnet, *Propriétés et Caractéristiques Des Matériaux De Construction (Properties and Characteristics of Building Materials)*, Le monteur, 2005.
[20] J.W. Cooley, J.W. Tukey, An algorithm for the machine calculation of complex Fourier series, *Mathematics of Computation* 19 (1965) 297–301.
[21] J. Max, *Méthodes et Techniques de Traitement du Signal et Application Aux Mesures Physiques (Methods and Techniques of Signal Processing and Application in the Physical Measurements)*, Masson & Cie, 1972.
[22] L. Bos, Caracterisation acoustique des parois épaisses périodiques dans les locaux industriels (Acoustic Characterisation of the Periodic Profiles Present in Industrial Rooms), Ph.D. Thesis, Universite Henri Poincaré, Nancy, 2006.